Contents list available at CBIORE journal website

International Journal of Renewable Energy Development

Journal homepage: https://ijred.cbiore.id

Research Article

Experimental investigation of a wildlife-safe origami-inspired reaction-type wind turbine for sustainable urban energy systems

Ahmad Sedaghat[1], Mohamad Hussein Farhat[2*], Bassem Djedi[3], Mohamad Iyad Al-Khiami[4], Mohamed El Badawy[1]

[1]*Department of Mechanical Engineering, College of Engineering, Australian University, Safat 13015, West Mishref, Kuwait*

[2]*Department of Electrical and Electronics Engineering, College of Engineering, Australian University, Safat 13015, West Mishref, Kuwait*

[3]*School of Aviation, Australian University, Safat 13015, West Mishref, Kuwait*

[4]*Department of Civil Engineering, College of Engineering, Australian University, Safat 13015, West Mishref, Kuwait*

Abstract. Small-scale wind turbines offer sustainable solutions for distributed renewable energy generation in urban environments. However, their deployment is often limited by concerns related to noise, visual impact, and risks to flying wildlife. This study presents an experimental investigation of a novel origami-inspired reaction-type wind turbine designed to improve urban compatibility through a compact, aesthetic, and bladeless configuration that enhances operational safety. Unlike conventional lift- or drag-based turbines, the proposed design operates based on a reaction force generated by redirecting axial inlet airflow into tangential outlet flow through internal nozzle conduits. Two miniature prototypes were fabricated using 3D printing with rotor diameters of 10 cm and 8 cm, both designed with a nozzle aspect ratio of unity and incorporating four inlet openings. The performance of the turbines was evaluated experimentally and theoretically under four operating conditions: free rotation, generator operation without load, fixed load operation, and variable load operation. Key performance parameters including cut-in wind speed, rotational speed, power output, and power coefficient were assessed through wind tunnel testing. The results demonstrate that the proposed origami wind turbine achieves a maximum power coefficient of $C_P=0.28$ at a tip speed ratio of $\lambda=1.21$, which is comparable to conventional small-scale turbines despite its bladeless configuration. Importantly, this study establishes that a reaction-type, bladeless turbine can simultaneously deliver competitive aerodynamic performance while significantly improving safety, reducing noise, and minimizing environmental impact. These findings highlight the strong potential of origami-inspired reaction-type wind turbines as viable and sustainable solutions for urban energy systems.

Keywords: Origami-inspired wind turbine; Reaction-type turbine; Bladeless wind turbine; Small-scale wind energy; Urban wind energy systems; Wildlife-safe design.

Received:19th Feb 2026; Revised: 27th March 2026; Accepted: 3rd May 2026; Available online: 8th May 2026

1. Introduction

Urban environments face increasing challenges, including rising energy demand, carbon emissions, sustainability requirements, and the need for compatible infrastructure. Environmental engineering solutions increasingly focus on integrating renewable energy technologies into cities while minimizing ecological disturbance, noise pollution, and visual impact. Small wind turbines (SWTs), typically defined as wind turbines with power production below 0.5 kW and rotor diameters below 1 meter, represent a promising approach for distributed renewable energy generation. These small turbines can be arranged in cascade wall configurations to provide appreciable cumulative power production while supporting decentralized clean energy systems. Their ability to generate electricity close to the point of consumption reduces reliance on centralized power grids and associated transmission infrastructure, contributing to more sustainable urban energy systems (Tayebi & Torabi, 2024).

In urban and suburban environments where space limitations and environmental considerations are critical, the compact size, relatively quiet operation, and modular nature of SWTs make them suitable candidates for electricity generation. Their scalability allows flexible deployment either individually or in arrays to meet varying energy demands while supporting sustainable city development. Additionally, SWTs provide valuable platforms for education and research related to renewable energy systems.

In this research, a novel SWT inspired by the common origami windmill (pinwheel) is proposed, with emphasis on improving urban compatibility and deployment safety. Most wind turbines developed to date are either drag-based or lift-based devices operating in vertical or horizontal orientations (Rolin & Porté-Agel, 2018). The proposed origami SWT introduces a bladeless and hub-less configuration that operates using reaction forces generated by redirecting airflow through internal nozzle-shaped conduits. This design eliminates exposed rotating blades, thereby improving operational safety, reducing noise emissions, and minimizing risks to urban wildlife

* Corresponding Author
Email: m.farhat@au.edu.kw (M.H.Farhat)

https://doi.org/10.61435/ijred.2026.62526
ISSN: 2252-4940/© 2026.The Author(s). Published by CBIORE

such as birds. Such design considerations are increasingly important for integrating renewable technologies into dense urban environments. However, limited studies have explored reaction-type wind turbine concepts with bladeless configurations, particularly for urban applications. Recent studies have also highlighted the potential of origami-inspired turbine designs for improving urban wind energy integration and scalability (Farhat *et al*., 2025).

The proposed concept may also complement solar energy generation in hot climates such as Kuwait, where environmental factors such as dust accumulation and high temperatures often reduce photovoltaic efficiency. Hybrid renewable approaches can therefore improve the resilience and sustainability of urban energy systems. This introduction also reviews the latest developments, challenges, and state-of-the-art technologies related to micro vertical axis wind turbines (VAWT) and horizontal axis wind turbines (HAWT) for urban environments and investigates their potential role in sustainable infrastructure (Dossena *et al*., 2015). These micro wind turbines are typically classified with larger power ratings of several kW and rotor diameters exceeding 2 meters.

Despite the limited diversity of HAWT configurations, VAWT designs have expanded rapidly with many alternative geometries and operational concepts. VAWTs are often considered suitable for urban applications due to their independence from wind direction, absence of yaw mechanisms, tolerance to turbulent flow conditions, and relatively low noise levels associated with lower tip speed ratios (TSR). Two main types of VAWTs exist: lift-based designs such as Darrieus turbines and drag-based designs such as Savonius turbines. Hybrid configurations combining both concepts have also been developed to improve self-starting capability.

A critical review of VAWT applications in urban environments highlighted inherent deficiencies, including low power coefficients and poor self-starting performance (Tayebi & Torabi, 2024). These limitations are partly associated with flow separation over aerofoils and low lift-to-drag ratios. Flow around VAWTs is inherently unsteady, producing distorted wake structures that may lead to dynamic stall at TSR values below 2 (Rolin & Porté-Agel, 2018). When multiple VAWTs are installed in arrays, blockage and wake interactions become significant, with blockage effects below 10% still producing measurable performance impacts (Dossena *et al*., 2015). Studies indicate that spacing equivalent to one rotor diameter is adequate for same-rotation turbine pairs (Ahmadi-Baloutaki *et al*., 2016).

Solidity is another important parameter influencing VAWT performance. Increasing solidity slightly improves maximum power coefficient at lower TSR values (Eboibi *et al*., 2016), while lower solidity provides flatter power coefficient curves across wider TSR ranges (Maeda *et al*., 2016). Variable pitch mechanisms have demonstrated improved power coefficients compared to fixed-pitch turbines (Elkhoury *et al*., 2015). Increasing blade number has been shown to influence wake asymmetry and velocity deficits downstream (Peng *et al*., 2016), while reducing blade number may negatively affect self-starting capability and rated power performance (Joo *et al*., 2015).

Wind speed fluctuations also affect turbine performance. Fluctuations within 7% of the mean wind speed show minimal impact, whereas fluctuations above 12% result in reduced unsteady power coefficients and energy yield (Danao *et al*., 2013). Computational studies on cambered aerofoils demonstrate that blades with 1.5% camber achieve improved cycle-averaged power coefficients under fluctuating conditions (Bausas & Danao, 2015).

Flexible blade concepts have also been explored, showing improved lift-to-drag ratios due to delayed flow separation (Wang *et al*., 2019). Trailing-edge flap integration improves control of flow separation and delays dynamic stall (Han *et al*., 2023). Large experimental datasets involving multiple VAWT configurations show that tip flow effects may promote flow reattachment at aspect ratios above 8 (Tong *et al*., 2023). Helical blade designs, although complex to manufacture, have been found to produce lower power coefficients compared to straight blade designs (Lee & Lim, 2015). Recent experimental investigations on flexible and rigid 3D-printed Savonius turbines with aerodynamic augmentation demonstrated significant improvements in performance and efficiency, particularly under urban wind conditions (Ghareeb *et al*., 2026).

HAWTs are lift-based turbines consisting of multiple blades mounted on a hub with yaw mechanisms. Compared to VAWTs, HAWTs generally achieve higher efficiencies and power outputs due to higher TSR operation. However, their use in urban environments presents challenges including visual impact, noise emissions, flicker effects, and safety concerns. Furthermore, highly turbulent urban wind conditions may reduce efficiency and increase structural loading variability (Castellani *et al*., 2018). Periodic wind speed variations have been shown to produce fluctuations in output power and mechanical loads (Castellani *et al*., 2019). Specialized experimental setups have been developed to better understand micro-HAWT performance under controlled conditions (Ajirlo *et al*., 2021).

To improve performance of small HAWTs for building integration, various augmentation approaches including diffusers and shrouds have been investigated (Rahmatian *et al*., 2022). Optimization methods have been applied to characterize diffuser-augmented designs (Vaz & Wood, 2016), while variable shroud geometries demonstrate power improvements of approximately 37% (Siavash *et al*., 2020). Blade shape optimization studies using both experimental and computational approaches have identified optimal configurations using blade element momentum (BEM) theory (Hsiao *et al*., 2013). Hybrid aerofoil blade designs have also been proposed for rooftop installations (Gaonkar & Hegde, 2022). Pitch control mechanisms have additionally been used to safely shut down turbines at cut-out wind speeds (Shuwa *et al*., 2020). A summary of the limitations of previous wind turbine technologies and how the present study addresses them is provided in Table 1.

Existing wind turbine technologies for urban applications include lift-based designs such as Darrieus turbines, which provide relatively high efficiency but suffer from poor self-starting capability and structural complexity, and drag-based designs such as Savonius turbines, which offer simplicity and reliable starting behaviour but are limited by low power coefficients. Micro horizontal axis wind turbines can achieve higher efficiencies; however, their application in urban environments is restricted due to noise emissions, safety concerns, and sensitivity to turbulent flow conditions. In contrast, the proposed origami-inspired reaction-type wind turbine introduces a bladeless configuration that enhances operational safety, reduces environmental impact, and maintains competitive performance for small-scale urban energy applications.

This research paper is organized as follows. Section 1 introduces the origami-inspired wind turbine concept and reviews recent developments in VAWT and HAWT technologies within the context of sustainable urban energy

Table 1
Summary of previous studies, their limitations, and how the present study addresses them.

Study Area	Key Findings	Limitations	How This Study Addresses Them
VAWTs in urban environments	Suitable for turbulent flows and omnidirectional wind	Low power coefficient, poor self-starting	Introduces reaction-based origami turbine improving startup and safety
Flow behaviour in VAWTs	Dynamic stall and wake interactions reduce performance	Unsteady aerodynamics limits efficiency	Uses internal flow redirection (axial → tangential) to stabilize operation
Solidity and blade effects	Influences Cp and TSR performance	Trade-off between efficiency and starting	Eliminates blades entirely (bladeless concept)
HAWTs in urban areas	Higher efficiency than VAWTs	Noise, visual impact, wildlife risk	Compact, aesthetic, wildlife-safe design
Augmented turbines (diffusers/shrouds)	Improve power output	Added complexity and cost	Simpler internal nozzle-based acceleration
Flexible/advanced blades	Delay separation, improve performance	Manufacturing complexity	Uses simple 3D-printed geometry

systems. Section 2 presents the origami concept and aesthetic features of the proposed design. Section 3 describes the experimental methodology, materials, and theoretical modelling including CFD simulations. Section 4 presents theoretical and experimental results under four operating scenarios. Section 5 discusses the results and associated correlations. Finally, Section 6 presents the conclusions.

2. An Origami Concept and Aesthetics Features

The familiar origami paper windmill, or pinwheel model, with below 10 cm rotor diameter brings back childhood memories of playing with this simple, wind-driven paper made toy. Most people take its operation for granted drag based operation but rarely consider how it works. By closely examining the rotation direction and analysing how the wind interacts with the paper windmill, the underlying reaction-type operation of this toy is realized.

The reaction-type operation is unique and is neither drag nor lift type wind turbine concept. These SWTs are aesthetically pleasing and seamlessly integrate with the overall design of the building. Additionally, the rotor and tower can be painted to match the building's colour scheme, enhancing visual harmony. Multiple rotors within a single rectangular frame can be installed on building roofs, as shown in Fig. 1. These designs allow for the inclusion of several rotors, thereby increasing the overall power output. The rotor cascades with a yaw mechanism can be arranged in alternating orientations within the frame to align with the optimal wind direction for enhanced performance. Fig. 1 depicts a sustainable building design that combines solar panels with these innovative SWTs, offering a comprehensive approach to renewable energy in urban settings. These design concepts seek to balance aesthetic appeal with the practical efficiency of wind energy and can supply off-grid charging stands for electric vehicles (EVs) and other indoor appliances.

3. Materials and Methods

3.1 3D Prints

A 3D printer with a dual extruder was used here to produce the origami wind turbine models. The printer allows maximum printable dimensions of 300 mm × 250 mm × 200mm and operates at an extruder temperature range up to 300 °C and

Fig 1. Overview of a building with hybrid renewable energy generation

Table 2
Technical specification of two origami rotor designs.

Model Name	Model Shape	Specification	Comments
Black Model		Length: 4 cm Inner Diameter: 10 cm Outer Diameter: 17 cm Inlet Nozzle Diameter: 3.5 cm Outlet Nozzle Diameter: 3.5 cm AR: 1	The origami wind turbine (100% model) started rotation with and without generator at the cut-in wind speed of 3.2 m/s (This is the minimum speed of the wind tunnel).
Green Model	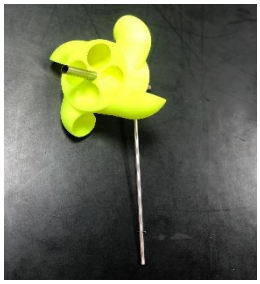	Length: 3.2 cm Inner Diameter: 8 cm Outer Diameter: 13.6 cm Inlet Nozzle Diameter: 2.8 cm Outlet Nozzle Diameter: 2.8 cm AR: 1	The origami wind turbine (80% model) started free rotation at the cut-in wind speed of 3.2 m/s and with the generator at the cut-in wind speed of 4.2 m/s.

diameter of 0.4 mm. The print speed can be adjusted from 10 mm/s to 150 mm/s. A support layer option was also enabled to help the models adhere to the platform. The black model took 12 hours and the green model 8 hours to be printed. Table 2 shows the specification of two origami designs, which were 3D printed.

3.2 The Wind Tunnel

The wind tunnel is an open type wind tunnel with a test section size of 292 mm in width, 292 mm in height, and 420 mm in length (GUNT, 2026). Air enters through a honeycomb mesh into the inlet nozzle of wind tunnel and passes through the transparent test section and then exit through a long diffuser section by the action of a 3.4 kW electric motor with either 230 V, 50 Hz single phase or 230 V, 60 Hz three phases. The overall dimensions of the wind tunnel are 2870 mm in length, 890 mm in width, and 1540 mm in height, with an approximate weight of 250 kg.

The open wind tunnel generates air speeds from 1.3 m/s and up to 25 m/s. The wind tunnel is equipped with a balance system that enables rotation of models within $\pm 180^{o}$ and measures lift and drag forces up to 4 N. An inclined tube manometer is used to measure air speed in the test section. A data acquisition system and a personal computer (PC) is used to measure and display values of air speed, lift and drag forces, moment, displacements and angles and the differential pressures using the device software.

3.3 Measurement Uncertainty Analysis

Measurement uncertainty was evaluated to ensure the reliability of the experimental results obtained from the wind tunnel tests. The main measured parameters include wind speed, rotational speed, voltage, and current. Wind speed was measured using the GUNT HM 170 open wind tunnel with an uncertainty of ±0.1 m/s. Rotational speed was measured using a digital tachometer with an uncertainty of ±1 rpm. Electrical measurements were obtained using digital multimeters, with voltage and current uncertainties of ±0.01 V and ±0.001 A, respectively. summary of the measurement uncertainties is provided in Table 3.

Table 3
Measurement uncertainties of experimental parameters

Parameter	Error Band	Uncertainty
Wind speed (m/s)	±0.1	±0.1
Rotational speed (rpm)	±1	±1
Voltage (V)	±0.01	±0.01
Current (A)	±0.001	±0.001

Based on the accuracy of the measuring instruments, the overall uncertainty in the calculated power output is low and within acceptable limits for small-scale wind turbine experiments. These uncertainties do not affect the observed performance trends or the comparative analysis presented in this study.

4. Theoretical Approach

The origami inspired wind turbine design operates by a reaction force that is created by changing direction of wind airstream from axial direction into tangential direction. The reaction force is governed using the linear momentum equation that is expressed by the second law of Newton in motion as follows (Cengel & Cimbala, 2024):

$$\sum \vec{F} = \frac{d}{dt}\left(\int \rho \vec{V} d\mho\right)_{CV} + \left(\int \rho \vec{V}(\vec{V}.\vec{n}) dA\right)_{CS} \quad (1)$$

Equation 1 is expressed in vector form in which, $\sum \vec{F}$ is the sum of all external forces, the term $\frac{d}{dt}\left(\int \rho \vec{V} d\mho\right)_{CV}$ expresses the time rate of change of linear momentum of the differential mass contents of the control volume (CV), and the term $\left(\int \rho \vec{V}(\vec{V}.\vec{n}) dA\right)_{CS}$ expresses the net exiting linear momentum out of the control surface (CS) by the mass flow rate. In Eq. 1, ρ is the density of air, $\vec{V}$ is the wind velocity vector, $d\mho$ is the

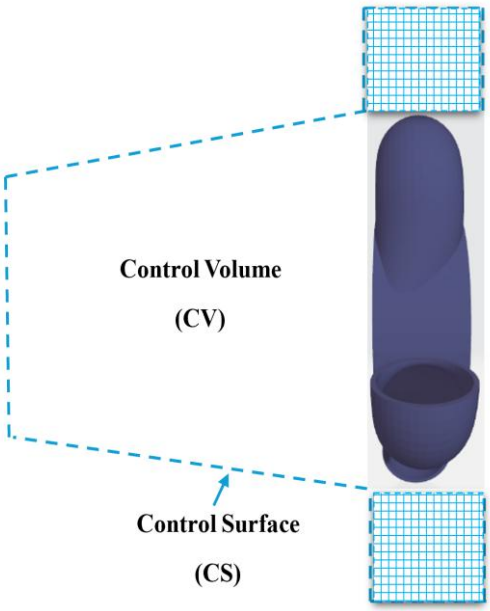

Fig 2. The CV and CS around the wind turbine.

differential volume, dA is the differential area, and $\vec{n}$ is the normal unit vector perpendicular to the control surfaces.

As shown in Fig. 2, the momentum equation is applied on a fixed CV around the wind turbine in a way that the airstream enters axially at the inlet of the wind turbine through a CS as the boundaries of the CV and airstream leaves the rotor tangentially perpendicular to the CS.

Considering the fixed CV, shown in Fig. 2, around the wind turbine, the time rate of the linear momentum $\left(\frac{d}{dt}\left(\int \rho\vec{V}d\mho\right)_{CV}\right)$ is omitted at steady-state condition. Also, the inlet wind direction is assumed one-dimensional in axial direction, and the outlet wind direction is assumed one-dimensional in tangential direction. Assuming the entire CS is at atmospheric pressure, then the second term $\left(\int \rho\vec{V}\left(\vec{V}.\vec{n}\right)dA\right)_{CS}$ in Eq. 1 is replaced by mass flow rate times inlet or outlet velocities. Hence, Eq. 1 is simplified for the steady-state two-dimensional flows as follows (Cengel & Cimbala, 2024):

$$\begin{aligned} F_a &= \dot{m}V_{in} \quad [N] \\ F_t &= \dot{m}V_{out} \quad [N] \end{aligned} \tag{2}$$

In Eq. 2, $\dot{m}$ is the mass flow rate, V_{in} is the inlet velocity and V_{out} is the outlet velocity. The external force, F_a, is the axial force that corresponds to the unfavourable thrust or drag force and must be minimised. However, the external force, F_t, is the favourable reaction force in tangential direction at the outlet of the rotor. A torque and a shaft power are generated by the tangential force. This shaft power rotates an electric generator and produces an electric output power. Hence, the tangential force, F_t, must be maximised to obtain the maximum output power. However, having the same inlet and outlet areas implies that both normal and tangential forces must be equals (i.e., $F_a = F_t$ when $AR = 1$). This is one of the limitations of the origami designs.

An experimental study on external flows around straight nozzle, tube, and diffuser sections indicated that the inlet/outlet velocities is different than anticipated internal flows and the outlet velocity of these geometries are usually smaller or equals to the freestream wind velocity (V_{wind}) (Ohya *et al.*, 2008). Therefore, for the new rotor design, a retarding factor, β, is introduced to account for energy loss and turbulence on the inlet and outlet of the 3D internal circular conduits. Hence, knowing the aspect ratio of unity ($AR = 1$) in the present designs that implies the inlet and outlet velocities must be equal according to the continuity equation, the inlet/outlet velocities and mass flow rates are corrected by the fixed retarding factor (β) as follows (Cengel & Cimbala, 2024):

$$\begin{aligned} V_{in} = V_{out} &= \beta V_{wind} \quad [m/s] \\ \dot{m} &= \beta\rho A_{in}V_{wind} = \beta\rho A_{out}V_{wind} \; [kg/s] \end{aligned} \tag{3}$$

The correcting factor β may also interpreted as the true aerodynamic performance of the origami rotor design by taking β proportion of the wind power and convert it completely to electrical power.

In wind turbine community, it is common to define a power coefficient as the ratio of the output generator electrical power or the rotor power to the input wind power as follows (Manwell *et al.*, 2024):

$$\begin{aligned} C_P &= \frac{P_R}{P_{wind}} \\ P_{wind} &= \frac{1}{2}\rho A_R V_{wind}^3 \; [W] \\ \lambda = TSR &= \frac{R.\omega}{V} \end{aligned} \tag{4}$$

In Eq. 4, A_R is usually used as the swept area by the rotor calculated by $A_R = \frac{\pi D^2}{4}$, but instead for the new Origami design the effective area for taking in wind speed is used, i.e., $A_R = A_{in} = \pi d_{in}^2$. The performance curves of wind turbines are usually expressed by $(C_P - \lambda)$ curves, with tip speed ratio (TSR) defined in Eq. 4.

Similarly, a torque coefficient is defined using Eq. 5 as follows (Manwell *et al.*, 2024):

$$C_Q = \frac{Q}{\frac{1}{2}\rho A_R V_{wind}^2 \frac{D}{2}} = \frac{8\beta^2 d_{out}^2}{D^2} = constant \tag{5}$$

Equation 5 indicates that the torque coefficient of the new wind turbine design is constant across all wind speeds. A constant

Table 4
Summary of experimental scenarios and measured parameters

Scenario	Configuration	Measured Parameters	Purpose
Scenario 1	Free rotation (no generator)	Rotational speed (RPM) vs wind speed	Determine cut-in speed and aerodynamic behavior
Scenario 2	Generator (no load)	Voltage vs wind speed	Evaluate generator coupling and inertia effects
Scenario 3	Generator with fixed load (LED)	Voltage, current, power, Cp, TSR	Assess performance under constant load
Scenario 4	Generator with variable load (5–5000 Ω)	Power, Cp, optimal resistance	Identify optimal operating conditions

torque coefficient indicates an aerodynamically optimised wind turbine design that can efficiently extract energy from the wind across a wide range of speeds, simplifying the control systems and providing consistent power output characteristics.

5. Results and discussion

Two origami rotor designs with 10 cm diameter (black model or 100% model) and 8 cm diameter (green model or 80% model) with aspect ratio of unity ($AR = 1$) were investigated using the described methodology both theoretically and experimentally using wind tunnel testing. The rotor models were fabricated using 3D printing techniques. Table 2 provides details of two origami rotor models investigated here.

Four experimental scenarios were investigated to evaluate the performance of the proposed wind turbine: free rotation without generator, operation with generator without load, operation with a fixed electrical load, and operation with variable electrical loads. These scenarios enable a comprehensive evaluation of aerodynamic behaviour, electrical output characteristics, and overall system performance under different operating conditions. The experimental scenarios investigated in this study are summarized in Table 4 for clarity.

5.1 Theoretical Results

Based on the mathematical modelling discussed in Section 4, the predicted output power and normal force are presented in Fig. 3 for the black and green models described in Table 2. In this analysis, it is assumed that for every 1 m/s increase in wind speed, the rotor speed increases by approximately 100 rpm. The calculations are performed using an aspect ratio of $AR = 1$ and correcting factor values of $\beta = 0.3$,0.4, and 0.5.

The theoretical power predictions are compared with the experimental results obtained under a constant electrical load (light-emitting diode, LED) at different wind speeds, as shown in Fig. 3a. The parameter β represents the fraction of wind energy extracted by the rotor. As observed in Fig. 3a, the

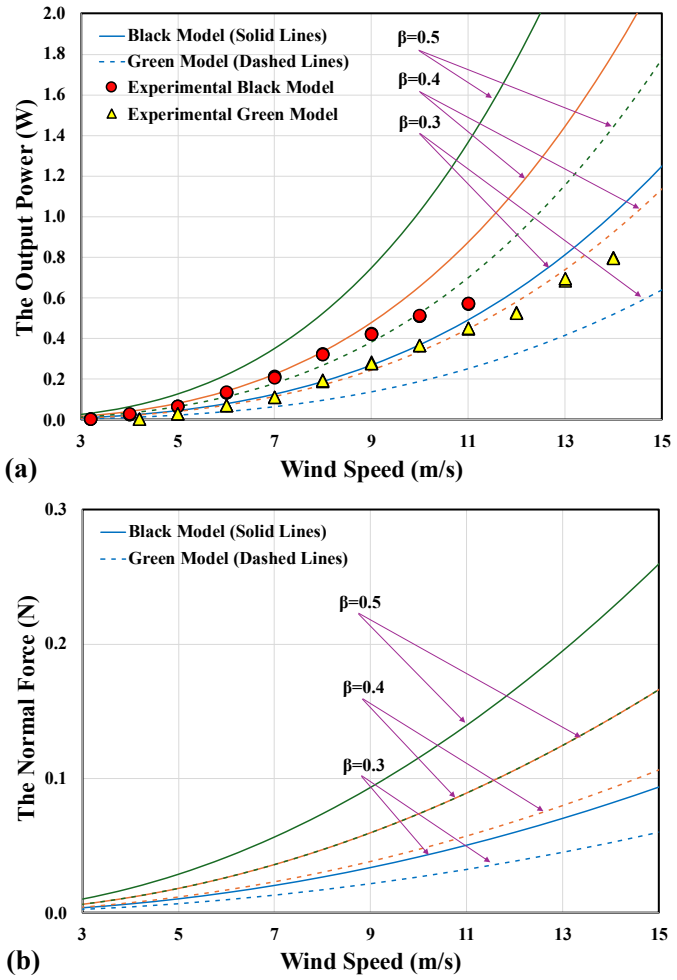

Fig 3. Theoretical performance of two origami wind turbines at different wind speeds and β=0.3, 0.4, and 0.5: (a) The output power performance, and (b) The normal force on the wind turbine mast.

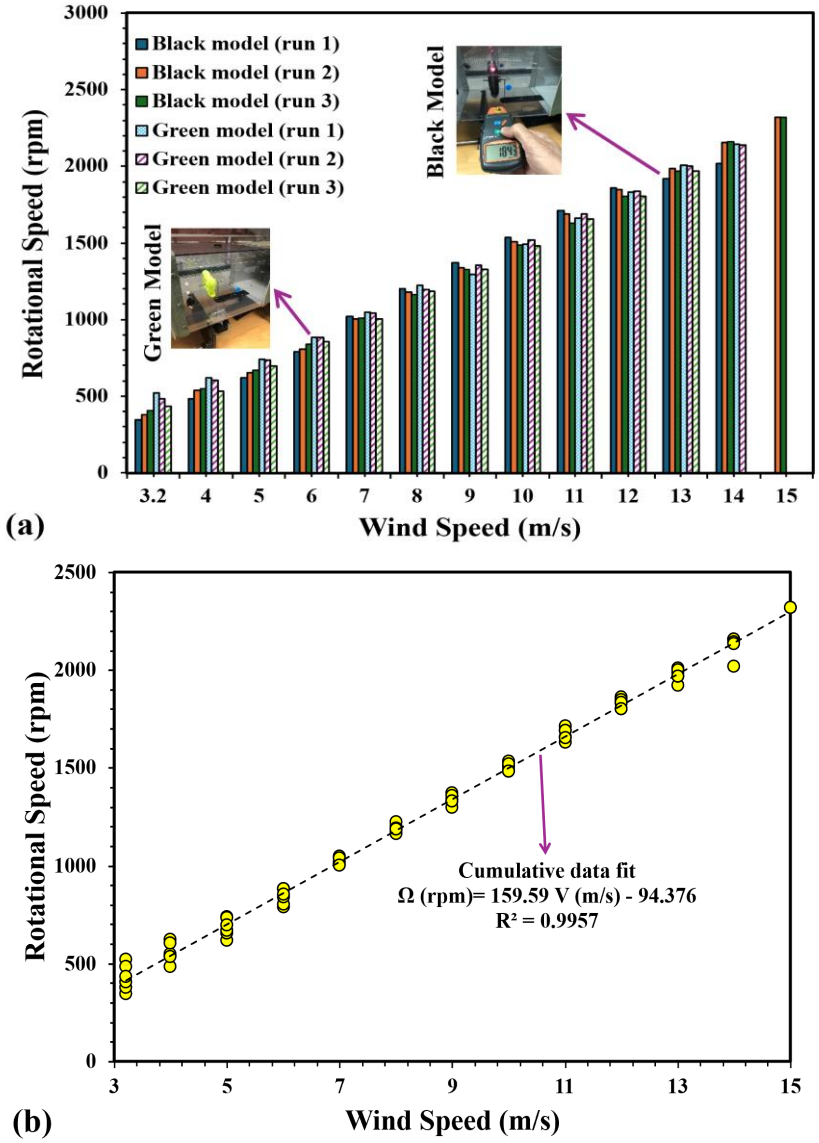

Fig 4. Free rotation performance of the black and green rotor models: (a) rotational speed versus wind speed, (b) cumulative data fit.

experimental power output of both the black and green rotors follows the theoretical curve corresponding to $\beta = 0.3$at wind speeds below approximately 11 m/s. At higher wind speeds, the experimental results deviate toward higher β values, indicating improved energy extraction. At the maximum wind speed of 25 m/s, the power output approaches the theoretical curve corresponding to $\beta = 0.4$.

The theoretical normal force results are presented in Fig. 3b. For $\beta = 0.3$at a wind speed of 10 m/s, the normal forces for the black and green models are 0.0416 N and 0.0266 N, respectively. At a wind speed of 25 m/s and $\beta = 0.4$, the normal forces increase to 0.2598 N and 0.1663 N for the black and green models, respectively.

This trend is consistent with classical wind energy theory, where power output increases with wind speed due to the cubic relationship between wind velocity and available energy (Manwell *et al.*, 2024). The improvement in effective β at higher wind speeds can also be attributed to reduced relative viscous losses and improved flow behavior at higher Reynolds numbers, which has been observed in small-scale wind turbine studies (Danao *et al.*, 2013).

5.2 Scenario 1: Experiments without Generator

In the first scenario, wind tunnel measurements are presented for three runs for both the black and green models, as shown in Fig. 4a. The rotational speeds of both models were measured using a tachometer, starting from the cut-in wind speed of 3.2 m/s and continuing up to 15 m/s. Fig. 4b shows that the rotational speed of both rotors varies linearly with wind speed, with a strong correlation indicated by an R-squared value of 0.9957 under free rotation condition.

In this scenario, the rotor was allowed to rotate freely on the mounted shaft at different wind tunnel speeds (see Fig. 4a). The black and green models, both with a nozzle aspect ratio of unity ($AR = 1$), begin rotating at the minimum wind tunnel speed of 3.2 m/s. A clear linear relationship between rotational speed and wind speed is observed (see Fig. 4b). The high R-squared value (0.9957) indicates that both rotors exhibit nearly identical rotational characteristics, and that the linear fit accurately represents the experimental data over the wind speed range of 3.2 to 15 m/s.

The observed linear relationship between rotational speed and wind speed is typical of low-load turbine operation and has

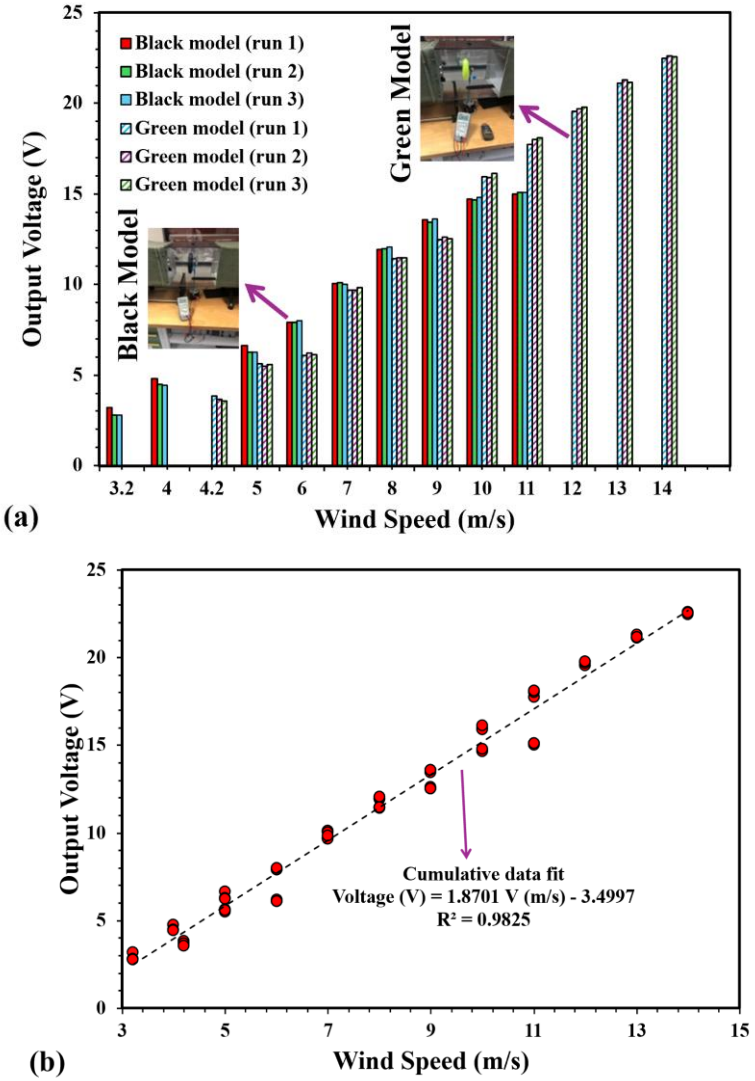

Fig 5. Open-circuit voltage performance of the black and green rotors mounted on the three-phase generator: (a) output voltage versus wind speed, (b) cumulative data fit.

been reported in experimental studies of small-scale wind turbines operating under minimal aerodynamic resistance (Danao *et al*., 2013).

5.3 Scenario 2: Experiments with Generator

In the second scenario, both the black and green models were connected to a three-phase generator without an electrical load to examine the effect of generator inertia on the cut-in wind speed and to measure the open-circuit voltage. Fig. 5a presents the open-circuit voltage generated by both wind turbine models at different wind speeds. As shown in Fig. 5b, both models exhibit similar trends between output voltage and wind speed, following a linear correlation with an R-squared value of 0.9825. For the black model, the maximum deviation occurs at a wind speed of 11 m/s, with an error of 13.31%. Similarly, for the green model, the maximum deviation is observed at a wind speed of 9 m/s, with an error of 6.28%. The maximum voltage of the three-phase generator is 24 V, and the green model achieved an average voltage of 22.55 V at a wind speed of 14 m/s. Overall, both models produce nearly identical voltage outputs at the same wind speed.

The linear voltage response with increasing wind speed reflects the proportional relationship between rotational speed and electromagnetic induction in small generators, which is consistent with established generator performance characteristics (Manwell *et al*., 2024).

5.4 Scenario 3: Experiments Using a Generator with a Fixed Load

In the third scenario, the black and green models were tested in the wind tunnel with a closed electrical circuit connected to a three-phase generator and a fixed load. A low-current LED lamp was used as the fixed load, allowing the output power to be determined by measuring the voltage and current across the load. Fig. 6 compares the power coefficient (C_P) of the black and green models as a function of the tip speed ratio (TSR).

The maximum average power coefficient ($C_P = 0.27$) was obtained at a TSR of 1.05 for the black model at a wind speed of 6 m/s. Therefore, the rated wind speed for the black model can be considered as 6 m/s. Similarly, the green model achieved a maximum average power coefficient of 0.26 at a TSR of 0.75 at a wind speed of 9 m/s, which can be considered its rated wind speed.

A comparison of the two models indicates that increasing rotor diameter shifts the rated wind speed to lower values. This characteristic is advantageous in low-wind-speed regions,

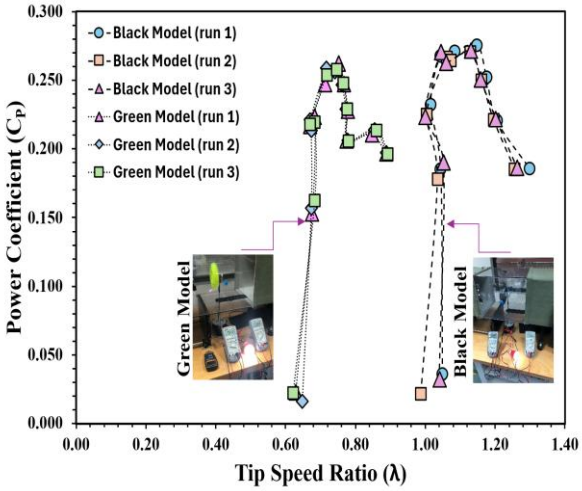

Fig 6. The characteristic performance of the black and green rotors: power coefficient versus tip speed ratio.

where larger rotors can achieve higher power output at lower wind speeds. The existence of an optimal tip speed ratio is a well-known characteristic of wind turbines, where maximum energy extraction occurs due to the balance between aerodynamic torque and rotational losses (Manwell *et al*., 2024). The relatively low optimal TSR observed in this study is consistent with drag-dominated or hybrid flow mechanisms typically reported for small-scale or unconventional turbine designs (Eboibi *et al*., 2016).

5.5 Scenario 4: Experiments Using both Generator and Variable Loads

In the fourth scenario, several resistors ranging from 5 Ω to 5000 Ω were used to assess the power performance of the black model under variable load conditions. The black model demonstrated superior performance in the previous scenarios and was therefore selected for further analysis. The power measurements were conducted using two multimeters to measure voltage and current across the loads. Fig. 7 shows the generator output electrical power at different wind speeds for various resistor values. In addition, Fig. 7 presents the power coefficient as a function of tip speed ratio (TSR) for different load conditions. For both cases, a third-order polynomial function provides an accurate fit to the maximum power curves.

In this scenario, only the black model was tested under variable load conditions using resistors ranging from 5 Ω to 5000 Ω connected to the three-phase generator. The performance results are presented in Fig. 7, where Fig. 7a illustrates the variation of output electrical power with wind speed for different resistor loads, while Fig. 7b shows the corresponding power coefficient as a function of TSR under the same loading conditions. As observed in Fig. 7a, the electrical power output increases with wind speed for all resistance values, with the 100 Ω load consistently yielding the highest power output across the tested range. Similarly, Fig. 7b demonstrates that the power coefficient varies with TSR and load, with the optimal performance again corresponding to the 100 Ω resistor.

A third-order polynomial fit accurately represents both the maximum power and power coefficient trends, with R^2values of 0.9983 and 0.9986, respectively. Under the optimal 100 Ω load, the maximum power coefficient of $C_P = 0.28$was achieved at a TSR of $\lambda = 1.21$and a rated wind speed of 8 m/s. In comparison, the third scenario with a fixed load produced a slightly lower maximum power coefficient of 0.27 at a TSR of 1.05 and a rated wind speed of 6 m/s. These results clearly indicate that optimizing the electrical load significantly enhances turbine performance.

The identification of an optimal electrical load reflects effective impedance matching between the generator and the external circuit, which is a common feature in small-scale wind energy systems (Eboibi *et al*., 2016). Similar improvements in power output through load optimization have been reported in experimental studies of micro wind turbines operating under variable electrical conditions (Ghareeb *et al*., 2026).

A consolidated summary of the key experimental findings is presented in Table 5. Although the present study is conducted on small-scale prototypes (8–10 cm rotor diameter), the underlying operating principle based on momentum redirection is inherently scalable. The governing equations (Eqs. 2–4) are independent of geometric scale and depend primarily on mass flow rate and velocity components, suggesting that similar aerodynamic behaviour can be achieved at larger sizes. However, scaling to real systems (0.5–1 m diameter) requires consideration of Reynolds number effects, structural integrity, and manufacturing constraints, particularly for maintaining internal nozzle geometry and minimizing flow losses. Future work will therefore focus on the experimental validation of larger-scale prototypes under real outdoor conditions.

The performance of the proposed origami wind turbine can be compared with existing small-scale wind turbine

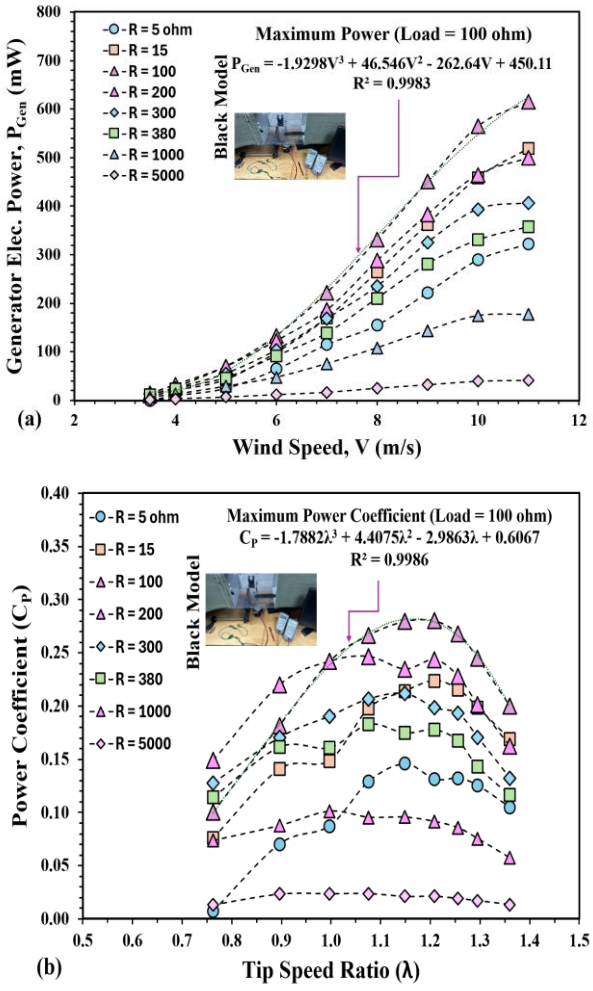

Fig 7. Performance of the black rotor under variable loads: (a) Output electrical power at different wind speeds using various resistors (b) Power coefficient versus tip speed ratio under different load conditions

Table 5
Key performance results of the origami wind turbine under different scenarios

Model	Scenario	Cut-in Speed (m/s)	Rated Wind Speed (m/s)	Max Cp	TSR at Max Cp	Key Observation
Black (10 cm)	Free rotation	3.2	–	–	–	Linear relationship between rotational speed and wind speed
Green (8 cm)	Free rotation	3.2	–	–	–	Similar trend to the black model
Black	Generator (no load)	3.2	–	–	–	Voltage increases linearly with wind speed
Green	Generator (no load)	4.2	–	–	–	Slight increase in cut-in speed due to generator inertia
Black	Fixed load	–	6	0.27	1.05	Optimal performance at relatively low wind speed
Green	Fixed load	–	9	0.26	0.75	Higher wind speed required for optimal performance
Black	Variable load	–	8	0.28	1.21	Maximum performance achieved at 100 Ω load

technologies reported in the literature. Conventional drag-based vertical axis wind turbines, such as Savonius rotors, typically achieve power coefficients in the range of 0.15–0.30, while lift-based turbines such as Darrieus designs can reach values up to 0.35–0.45 under optimal conditions (Manwell *et al.*, 2024). The present origami-inspired reaction-type turbine achieved a maximum power coefficient of approximately 0.28, which is comparable to drag-based turbines while offering additional advantages such as improved safety, reduced noise, and elimination of exposed rotating blades.

Unlike conventional designs that rely on lift or drag forces, the proposed turbine operates based on momentum redirection, representing a distinct operational mechanism. Similar alternative flow-based concepts have been explored in recent studies on unconventional wind energy systems for urban applications (Tayebi & Torabi, 2024). Although the efficiency is lower than that of high-performance lift-based turbines, the proposed design demonstrates competitive performance for urban environments where safety, compactness, and environmental compatibility are critical considerations.

6. Conclusions

Two small-scale laboratory models of 10 cm (black model) and 8 cm (green model) rotor diameters were manufactured using 3D printing and experimentally investigated in a subsonic wind tunnel at Australian University (AU), Kuwait. These models will be scaled up to rotor diameters in the range of 0.5 m to 1.0 m for field testing. This scaling will enable the investigation of real-world aerodynamic performance, structural behaviour, and environmental interaction, supporting the practical deployment of origami-inspired wind turbines in urban energy systems. Four experimental scenarios were conducted in the wind tunnel, and the main conclusions are summarized as follows:

- In the first scenario, both black and green models, initiated rotation at the minimum wind tunnel speed, with a cut-in wind speed of 3.2 m/s and exhibited a linear relationship between rotational speed and wind speed.
- In the second scenario, the black model connected to the three-phase generator started operating at a cut-in wind speed of 3.2 m/s, while the green model required a slightly higher wind speed of 4.2 m/s. Both models exhibited a linear correlation between rotational speed and generated voltage with increasing wind speed.
- In the third scenario, distinct performance characteristics were observed for both models under fixed load conditions. The black model demonstrated superior performance, achieving a maximum power coefficient of 0.27 at a TSR of 1.05 and a rated wind speed of 6 m/s. In contrast, the green model achieved a maximum power coefficient of 0.26 at a TSR of 0.75 at a higher rated wind speed of 9 m/s.
- In the fourth scenario, the black model was evaluated under variable resistor loads ranging from 5 Ω to 5000 Ω. The optimal load of 100 Ω resulted in a maximum power coefficient of 0.28 at a TSR of 1.21 and a rated wind speed of 8 m/s, demonstrating that electrical load optimization significantly enhances turbine performance.

Future work will focus on scaling the proposed origami wind turbine to larger sizes and evaluating its performance under real outdoor conditions. Additional studies will investigate optimization of rotor geometry and internal nozzle design, as well as structural durability and integration with hybrid renewable energy systems for urban applications.

Declaration of generative AI and AI-assisted technologies in the writing process

During the preparation of this work the authors used ChatGPT to improve the language. After using this tool, the authors reviewed and edited the content as needed and take(s) full responsibility for the content of the publication.

Acknowledgements

We would like to acknowledge the support of all faculty and staff at the Australian University (AU) of Kuwait who contributed to this research.

References

Ahmadi-Baloutaki, M., Carriveau, R., & Ting, D. S. (2016). A wind tunnel study on the aerodynamic interaction of vertical axis wind turbines in array configurations. *Renewable Energy*, *96*, 904-913. https://doi.org/10.1016/j.renene.2016.05.060Get rights and content

Ajirlo, K. S., Tari, P. H., Gharali, K., & Zandi, M. (2021). Development of a wind turbine simulator to design and test micro HAWTs. *Sustainable energy technologies and assessments*, *43*, 100900. https://doi.org/10.1016/j.seta.2020.100900

Bausas, M. D., & Danao, L. A. M. (2015). The aerodynamics of a camber-bladed vertical axis wind turbine in unsteady wind. *Energy*, *93*, 1155-1164. https://doi.org/10.1016/j.energy.2015.09.120

Castellani, F., Astolfi, D., Becchetti, M., Berno, F., Cianetti, F., & Cetrini, A. (2018). Experimental and numerical vibrational analysis of a horizontal-axis micro-wind turbine. *Energies*, *11*(2), 456. https://doi.org/10.3390/en11020456

Castellani, F., Astolfi, D., Natili, F., & Mari, F. (2019). The yawing behavior of horizontal-axis wind turbines: A numerical and experimental analysis. *Machines*, *7*(1), 15. https://doi.org/10.3390/machines7010015

Cengel, Y., & Cimbala, J. (2024). *Ebook: Fluid mechanics fundamentals and applications (si units)*. McGraw Hill.

Danao, L. A., Eboibi, O., & Howell, R. (2013). An experimental investigation into the influence of unsteady wind on the performance of a vertical axis wind turbine. *Applied Energy*, *107*, 403-411. https://doi.org/10.1016/j.apenergy.2013.02.012

Dossena, V., Persico, G., Paradiso, B., Battisti, L., Dell'Anna, S., Brighenti, A., & Benini, E. (2015). An experimental study of the aerodynamics and performance of a vertical axis wind turbine in a confined and unconfined environment. *Journal of Energy Resources Technology*, *137*(5), 051207. https://doi.org/10.1115/1.4030448

Eboibi, O., Danao, L. A. M., & Howell, R. J. (2016). Experimental investigation of the influence of solidity on the performance and flow field aerodynamics of vertical axis wind turbines at low Reynolds numbers. *Renewable Energy*, *92*, 474-483. https://doi.org/10.1016/j.renene.2016.02.028

Elkhoury, M., Kiwata, T., & Aoun, E. (2015). Experimental and numerical investigation of a three-dimensional vertical-axis wind turbine with variable-pitch. *Journal of wind engineering and Industrial aerodynamics*, *139*, 111-123. https://doi.org/10.1016/j.jweia.2015.01.004

Farhat, M. H., Mehdizadeh, A., Sedaghat, A., El Badawy, M., Djedi, B., Al-Khiami, M. I., Mostafaeipour, A., & Nazififard, M. (2025). Origami-inspired urban wind turbines: Scalable bladeless designs for decentralized renewable energy. *Green Technologies and Sustainability*, 100253. https://doi.org/10.1016/j.grets.2025.100253

Gaonkar, R. U., & Hegde, R. N. (2022). An investigation on the performance and viability of a hybrid twisted blade profile for a horizontal axis micro wind turbine. *Materials Today: Proceedings*, *49*, 1200-1209. https://doi.org/10.1016/j.matpr.2021.06.288

Ghareeb, N., Sedaghat, A., Farhat, M. H., Mehdizadeh, A., Ashtian Malayer, M., El Badawy, M., & Irannezhad, M. (2026). Experimental study on flexible and rigid 3D-Printed Savonius vertical axis wind turbines with aerodynamic augmentation. *Wind Engineering*, 0309524X261443931. https://doi.org/10.1177/0309524X261443931

GUNT. (2026). *HM 170 Open wind tunnel*. Retrieved 25 April 2026 from https://www.gunt.de/en/products/open-wind-tunnel/070.17000/hm170/glct-1:pa-148:pr-769

Han, Z., Chen, H., Chen, Y., Su, J., Zhou, D., Zhu, H., Xia, T., & Tu, J. (2023). Aerodynamic performance optimization of vertical axis wind turbine with straight blades based on synergic control of pitch and flap. *Sustainable energy technologies and assessments*, *57*, 103250. https://doi.org/10.1016/j.seta.2023.103250

Hsiao, F.-B., Bai, C.-J., & Chong, W.-T. (2013). The performance test of three different horizontal axis wind turbine (HAWT) blade shapes using experimental and numerical methods. *Energies*, *6*(6), 2784-2803. https://doi.org/10.3390/en6062784

Joo, S., Choi, H., & Lee, J. (2015). Aerodynamic characteristics of two-bladed H-Darrieus at various solidities and rotating speeds. *Energy*, *90*, 439-451. https://doi.org/10.1016/j.energy.2015.07.051

Lee, Y.-T., & Lim, H.-C. (2015). Numerical study of the aerodynamic performance of a 500 W Darrieus-type vertical-axis wind turbine. *Renewable Energy*, *83*, 407-415. https://doi.org/10.1016/j.renene.2015.04.043

Maeda, T., Kamada, Y., Murata, J., Shimizu, K., Ogasawara, T., Nakai, A., & Kasuya, T. (2016). Effect of solidity on aerodynamic forces around straight-bladed vertical axis wind turbine by wind tunnel experiments (depending on number of blades). *Renewable Energy*, *96*, 928-939. https://doi.org/10.1016/j.renene.2016.05.054

Manwell, J. F., Branlard, E., McGowan, J. G., & Ram, B. (2024). *Wind energy explained: on land and offshore*. John Wiley & Sons.

Ohya, Y., Karasudani, T., Sakurai, A., Abe, K.-i., & Inoue, M. (2008). Development of a shrouded wind turbine with a flanged diffuser. *Journal of wind engineering and Industrial aerodynamics*, *96*(5), 524-539. https://doi.org/10.1016/j.jweia.2008.01.006

Peng, H., Lam, H., & Lee, C. (2016). Investigation into the wake aerodynamics of a five-straight-bladed vertical axis wind turbine by wind tunnel tests. *Journal of wind engineering and Industrial aerodynamics*, *155*, 23-35. https://doi.org/10.1016/j.jweia.2016.05.003

Rahmatian, M. A., Tari, P. H., Mojaddam, M., & Majidi, S. (2022). Numerical and experimental study of the ducted diffuser effect on improving the aerodynamic performance of a micro horizontal axis wind turbine. *Energy*, *245*, 123267. https://doi.org/10.1016/j.energy.2022.123267

Rolin, V. F., & Porté-Agel, F. (2018). Experimental investigation of vertical-axis wind-turbine wakes in boundary layer flow. *Renewable Energy*, *118*, 1-13. https://doi.org/10.1016/j.renene.2017.10.105

Shuwa, M., Ngala, G., & El-jummah, A. (2020). Performance analysis of horizontal axis wind turbine using variable blade pitch control mechanism. *Arid Zone Journal of Engineering, Technology and Environment*, *16*(1), 179-187.

Siavash, N. K., Najafi, G., Hashjin, T. T., Ghobadian, B., & Mahmoodi, E. (2020). An innovative variable shroud for micro wind turbines. *Renewable Energy*, *145*, 1061-1072. https://doi.org/10.1016/j.renene.2019.06.098

Tayebi, A., & Torabi, F. (2024). Flow control techniques to improve the aerodynamic performance of Darrieus vertical axis wind turbines: A critical review. *Journal of wind engineering and Industrial aerodynamics*, *252*, 105820. https://doi.org/10.1016/j.jweia.2024.105820

Tong, G., Yang, S., Li, Y., & Feng, F. (2023). Effects of blade tip flow on aerodynamic characteristics of straight-bladed vertical axis wind turbines. *Energy*, *283*, 129105. https://doi.org/10.1016/j.energy.2023.129105

Vaz, J. R., & Wood, D. H. (2016). Aerodynamic optimization of the blades of diffuser-augmented wind turbines. *Energy Conversion and Management*, *123*, 35-45. https://doi.org/10.1016/j.enconman.2016.06.015

Wang, Y., Tong, H., Sima, H., Wang, J., Sun, J., & Huang, D. (2019). Experimental study on aerodynamic performance of deformable blade for vertical axis wind turbine. *Energy*, *181*, 187-201. https://doi.org/10.1016/j.energy.2019.03.181